Probing entropic uncertainty and quantum correlations in a quadruple quantum dot device for two charge qubits

Hao Wang(汪浩)[†]

Shanghai Normal University Tianhua College, Shanghai 201815, *China*

(Received 8 September 2025; revised manuscript received 11 November 2025; accepted manuscript online 14 November 2025)

We analyze the quantum correlations, the quantum-memory-assisted entropic uncertainty (QMA-EUR), and its lower bound in a quadruple quantum dot device for two charge qubits. Herein, we select incompatible Pauli operators $\hat{\sigma}_x$ and $\hat{\sigma}_z$ as a pair of observables of interest for the measurement of particle A, and the uncertainty can be predicted from the entanglement of particle A with quantum memory B. We explore the dynamics of quantum discord and QMA-EUR, taking into account the effects of electron temperature, energy offsets, tunneling coupling, and the strength of coupling (i.e., the Coulomb interaction between electrons). Interestingly, our results indicate that there are certain adjustable parameters that can be tuned to suppress the entropy uncertainty bound and enhance quantum correlations.

Keywords: semiconductor charge qubits, entropy uncertainty relation, lower bound, quantum discord, quantum memory

PACS: 03.65.Yz, 03.65.Ta, 42.50.Lc

DOI: 10.1088/1674-1056/ae1f7c **CSTR:** 32038.14.CPB.ae1f7c

1. Introduction

Heisenberg's uncertainty principle[1] is widely regarded as one of the most fundamental features of the quantum world, which is fundamentally distinct from the classical world. Subsequently, based on Heisenberg's ideas related to the momentum and position measured for a particle, Kennard[2] formulated the first uncertainty relation in terms of the product of standard deviations, i.e., $\Delta x\Delta p_x \geq \hbar/2$. Later, this relation was generalized by Robertson[3] to accommodate two arbitrary observables $\hat{Q}$ and $\hat{R}$ as

$$\Delta\hat{Q}\Delta\hat{R} \geq \frac{1}{2}\left|\langle\psi|\left[\hat{Q},\hat{R}\right]|\psi\rangle\right|. \tag{1}$$

Notably, this uncertainty bound is state dependent, and it becomes a trivial result when the state $|\psi\rangle$ yields a zero-expectation value for the commutator $\left[\hat{Q},\hat{R}\right]$. Afterwards, to eliminate this defect, Deutsch[4] and Kraus[5] put forward the entropic uncertainty relation (EUR) in terms of Shannon entropy, and Maassen and Uffink[6] improved it into the form

$$\mathcal{H}\left(\hat{Q}\right)+\mathcal{H}\left(\hat{R}\right) \geq \log_2\frac{1}{c}, \tag{2}$$

where $\mathcal{H}\left(\hat{\mathcal{O}}\right) = -\sum_i p_i\left(\hat{\mathcal{O}}\right)\log_2 p_i\left(\hat{\mathcal{O}}\right)$ is the Shannon entropy of the observables $\hat{\mathcal{O}} \in \{\hat{Q},\hat{R}\}$, $p_i\left(\hat{\mathcal{O}}\right) = \left\langle\psi_i^{\hat{\mathcal{O}}}\middle|\hat{\rho}\middle|\psi_i^{\hat{\mathcal{O}}}\right\rangle$ represents the probability of measuring the observable $\hat{\mathcal{O}}$ on state $\hat{\rho}$ with the ith outcome and $c = \max_{j,k}\left|\left\langle\psi_j^{\hat{Q}}|\psi_k^{\hat{R}}\right\rangle\right|^2$ stands for the maximum overlap between any two eigenvectors $\left|\psi_j^{\hat{Q}}\right\rangle$ and $\left|\psi_k^{\hat{R}}\right\rangle$. The benefit of Eq. (2) lies in the fact that its lower bound depends only on measured observables, i.e., a state-independent quantity, rather than the one provided by Eq. (1).

The desire to obtain higher measurement precision has spurred further refinement of the uncertainty relation. Recently, Renes *et al.*[7] and Berta *et al.*[8] have made notable progress in this field: they studied a bipartite system, A and B, in which one (A) performs measurement operations while the other (B) serves as a quantum memory. The quantum-memory-assisted entropy uncertainty relation (QMA-EUR) can be expressed as

$$\mathcal{S}\left(\hat{Q}|B\right)+\mathcal{S}\left(\hat{R}|B\right) \geq \mathcal{S}\left(A|B\right)+\log_2\frac{1}{c}, \tag{3}$$

where $\mathcal{S}\left(\hat{\mathcal{O}}|B\right) = \mathcal{S}\left(\hat{\rho}_{\hat{\mathcal{O}}B}\right)-\mathcal{S}\left(\hat{\rho}_B\right)$ is the conditional von Neumann entropy of the post-measurement outcomes (after is measured) with $\mathcal{S}\left(\hat{\rho}\right) = -\mathrm{Tr}\left(\hat{\rho}\log_2\hat{\rho}\right)$ for density matrix $\hat{\rho}$. $\hat{\rho}_{AB}$ and $\hat{\rho}_B$ are the density matrices for the whole system and subsystem B. $\mathcal{S}\left(A|B\right) = \mathcal{S}\left(\hat{\rho}_{AB}\right)-\mathcal{S}\left(\hat{\rho}_B\right)$ is the conditional von Neumann entropy of $\hat{\rho}_{AB}$ with $\hat{\rho}_B = -\mathrm{Tr}_A\left(\hat{\rho}_{AB}\right)$ being the reduced state of the memory particle B. The QMA-EUR is of profound significance because it establishes that known quantum information to be encoded in a quantum memory can reduce or eliminate the uncertainty associated with the measurement outcomes of another particle entangled with the quantum memory. Li *et al.*[8] and Prevedel *et al.*[9] experimentally demonstrated the QMA-EUR via two back-to-back all-optical configurations. Subsequently, different aspects of quantum memory have been addressed in Refs. [10–15]. Entropic uncertainty relations have been demonstrated to have profound implications for the security of cryptographic protocols,[16,17]

[†]Corresponding author. E-mail: shnuwh@163.com

© 2026 Chinese Physical Society and IOP Publishing Ltd. All rights, including for text and data mining, AI training, and similar technologies, are reserved.

CPB Online In-Press

foundational principles of thermodynamics,[18] theoretical framework of entanglement,[19,20] and quantum metrology and measurements.[21–25]

A quadruple quantum dot device was fabricated in a GaAs/AlGaAs heterostructure containing a two-dimensional electron gas, as shown in Fig. 1. The experimental implementation of the model has been thoroughly examined in Ref. [26]. The choice of using the AlGaAs/GaAs model is well founded. The electron occupation in the double quantum dot (DQD) can be precisely tuned by applying bias voltages to a set of Schottky gates. This solid-state device is highly scalable and seamlessly integrates with existing semiconductor technology. It offers precise manipulation and control of quantum states, features a well-defined energy spectrum, and allows the interactions between electron–electron and tunneling coupling between DQDs to be tuned. Furthermore, the quadruple quantum dot system provides a practical and scalable platform for implementing qubits in quantum information processing.

In this article, we perform rigorous investigations into quantum memory, which can in principle be stored in a quadruple quantum dot device tailored for two charge qubits. This paper is organized as follows. In Section 2, we describe the Hamiltonian of a quadruple quantum dot device for two charge qubits, deriving the eigenvalues, corresponding eigenstates, and temperature-dependent density matrix. In Section 3, we formally present the definition of QMA-EUR, together with its lower bound and degree of tightness. In Section 4, we briefly expound the correlation between the entanglement of formation (EoF) and standard quantum discord (QD). In Section 5, we offer an elaboration of the results. In Section 6, our conclusions are summarized.

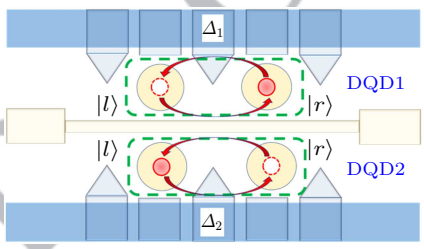


Fig. 1. Schematic representation of a quadruple quantum dot device for two charge qubits.

2. Semiconductor charge qubits and theoretical description

We consider a system of two charge qubits fabricated in an AlGaAs/GaAs heterostructure (see Fig. 1), each containing an excess electron in an orbital of either the left $|l\rangle_i$ or right $|r\rangle_i$ dot of the i-th semiconductor DQD ($i=1,2$).[27–30] The Hamiltonian of such a system reads

$$\hat{\mathcal{H}} = \frac{1}{2}\sum_i \left(\varepsilon_i \sigma_z^{(i)} + \Delta_i \sigma_x^{(i)}\right) + \frac{J}{4}\sigma_z^{(1)} \otimes \sigma_z^{(2)}, \tag{4}$$

where $\sigma_{x,y,z}^{(i)}$ are the Pauli matrices of the i-th qubit, ε_i parameters describe the energy offsets of the electronic levels, Δ_i refers to the tunneling coupling, and $J(>0)$ denotes the strength of the coupling within each DQD. Considering $\sigma_z = |l\rangle\langle l| - |r\rangle\langle r|$ and $\sigma_x = |l\rangle\langle r| + |r\rangle\langle l|$, the matrix form of Hamiltonian (1), written in the positional basis of the coupled molecules $\{|ll\rangle, |lr\rangle, |rl\rangle, |rr\rangle\}$, is given by

$$\hat{\mathcal{H}}_s = \begin{pmatrix} \frac{\varepsilon_1+\varepsilon_2}{2}+\frac{J}{4} & \frac{\Delta_2}{2} & \frac{\Delta_1}{2} & 0 \\ \frac{\Delta_2}{2} & \frac{\varepsilon_1-\varepsilon_2}{2}-\frac{J}{4} & \frac{J}{4} & \frac{\varepsilon_1}{2} \\ \frac{\Delta_1}{2} & \frac{J}{4} & -\frac{\varepsilon_1-\varepsilon_2}{2}-\frac{J}{4} & \frac{\Delta_2}{2} \\ 0 & \frac{\Delta_1}{2} & \frac{\Delta_2}{2} & \frac{\varepsilon_1+\varepsilon_2}{2}-\frac{J}{4} \end{pmatrix}. \tag{5}$$

Let us consider the computational basis of one qubit. In this basis, the Hadamard transformation $\hat{\mathcal{H}}$ can be represented by the 2×2 matrix

$$\tilde{\mathcal{H}} = \frac{1}{\sqrt{2}}\begin{pmatrix} 1 & 1 \\ 1 & -1 \end{pmatrix}. \tag{6}$$

Performing the double Hadamard transformation $\tilde{\mathcal{H}} = \tilde{\mathcal{H}} \otimes \tilde{\mathcal{H}}$ and taking into account[31]

$$\hat{\mathcal{H}}_{\mathrm{X}} = \tilde{\mathcal{H}}\hat{\mathcal{H}}_s\tilde{\mathcal{H}}^{\dagger}. \tag{7}$$

At full resonance, when $\varepsilon_1 = \varepsilon_2 = 0$, we derive the X-Hamiltonian matrix

$$\hat{\mathcal{H}}_{\mathrm{X}} = \begin{pmatrix} \Delta_+ & 0 & 0 & \frac{J}{4} \\ 0 & \Delta_- & \frac{J}{4} & 0 \\ 0 & \frac{J}{4} & -\Delta_- & 0 \\ \frac{J}{4} & 0 & 0 & -\Delta_+ \end{pmatrix}, \tag{8}$$

where $\Delta_\pm = \frac{1}{2}(\Delta_1 \pm \Delta_2)$. Hence, we obtain the following eigenvalues via diagonalization of the coupled semiconductor charge qubits.

$$\begin{aligned} E_1 &= -\frac{1}{4}\sqrt{J^2+16\Delta_-^2}, \\ E_2 &= \frac{1}{4}\sqrt{J^2+16\Delta_-^2}, \\ E_3 &= -\frac{1}{4}\sqrt{J^2+16\Delta_+^2}, \\ E_4 &= \frac{1}{4}\sqrt{J^2+16\Delta_+^2}, \end{aligned} \tag{9}$$

where their corresponding eigenstates in terms of the standard basis $\{|ll\rangle, |lr\rangle, |rl\rangle, |rr\rangle\}$ are given, respectively, by

$$\begin{aligned} |\psi_1\rangle &= \frac{1}{\sqrt{1+\alpha_-^2}}\left(\alpha_- |lr\rangle + |rl\rangle\right), \\ |\psi_2\rangle &= \frac{1}{\sqrt{1+\alpha_+^2}}\left(\alpha_+ |lr\rangle + |rl\rangle\right), \end{aligned}$$

Online In-Press

$$|\psi_3\rangle = \frac{1}{\sqrt{1+\beta_-^2}}\left(\beta_- |ll\rangle + |rr\rangle\right),$$
$$|\psi_4\rangle = \frac{1}{\sqrt{1+\beta_+^2}}\left(\beta_+ |ll\rangle + |rr\rangle\right), \tag{10}$$

with

$$\alpha_\pm = \frac{1}{J}\left(4\Delta_- \pm \sqrt{J^2+\Delta_-^2}\right),$$
$$\beta_\pm = \frac{1}{J}\left(4\Delta_+ \pm \sqrt{J^2+\Delta_+^2}\right).$$

The thermal density matrix of the system is given by the Gibbs state

$$\hat{\rho}(T) = \frac{1}{\mathcal{Z}}\exp\left(-\beta\hat{\mathcal{H}}_{\mathrm{X}}\right), \tag{11}$$

where $\beta = 1/k_{\mathrm{B}}T$ and $\mathcal{Z}$ are the partition function. The Boltzmann constant k_{B} is set to 1 in this work. The thermal density matrix $\hat{\rho}(T)$ can be analytically derived by using the spectral decomposition of the Hamiltonian (10). The density matrix takes the following form:

$$\hat{\rho}(T) = \frac{1}{\mathcal{Z}}\begin{pmatrix} \hat{\rho}_{11} & 0 & 0 & \hat{\rho}_{14} \\ 0 & \hat{\rho}_{22} & \hat{\rho}_{23} & 0 \\ 0 & \hat{\rho}_{32} & \hat{\rho}_{33} & 0 \\ \hat{\rho}_{41} & 0 & 0 & \hat{\rho}_{44} \end{pmatrix}, \tag{12}$$

where the corresponding entries are provided by

$$\hat{\rho}_{11} = \frac{1}{2\mathcal{Z}}\mathrm{e}^{-\beta(E_3+E_4)}\left[\mathrm{e}^{\beta E_4}(1-4\Lambda_+) + \mathrm{e}^{\beta E_3}(1+4\Lambda_+)\right],$$
$$\hat{\rho}_{22} = \frac{1}{2\mathcal{Z}}\mathrm{e}^{-\beta(E_1+E_2)}\left[\mathrm{e}^{\beta E_2}(1-4\Lambda_-) + \mathrm{e}^{\beta E_1}(1+4\Lambda_-)\right],$$
$$\hat{\rho}_{33} = \frac{1}{2\mathcal{Z}}\mathrm{e}^{-\beta(E_1+E_2)}\left[\mathrm{e}^{\beta E_1}(1-4\Lambda_-) + \mathrm{e}^{\beta E_2}(1+4\Lambda_-)\right],$$
$$\hat{\rho}_{44} = \frac{1}{2\mathcal{Z}}\mathrm{e}^{-\beta(E_3+E_4)}\left[\mathrm{e}^{\beta E_3}(1-4\Lambda_+) + \mathrm{e}^{\beta E_4}(1+4\Lambda_+)\right],$$
$$\hat{\rho}_{14} = \hat{\rho}_{41} = \frac{1}{2\mathcal{Z}}\left(\mathrm{e}^{-\beta E_4} - \mathrm{e}^{-\beta E_3}\right)\Gamma_+,$$
$$\hat{\rho}_{23} = \hat{\rho}_{32} = \frac{1}{2\mathcal{Z}}\left(\mathrm{e}^{-\beta E_2} - \mathrm{e}^{-\beta E_1}\right)\Gamma_-, \tag{13}$$

where

$$\Lambda_\pm = \frac{\Delta_\pm}{\sqrt{J^2+16\Delta_\pm^2}}, \quad \Gamma_\pm = \frac{J}{\sqrt{J^2+16\Delta_\pm^2}}$$

and the partition function

$$\mathcal{Z} = 2\Big[\cosh\left(\beta\sqrt{J^2+16\Delta_-^2}/4\right) + \cosh\left(\beta\sqrt{J^2+16\Delta_+^2}/4\right)\Big].$$

3. Quantum memory assisted entropic uncertainty relation

To study the dynamic behavior of entropic uncertainty QMA-EUR in our theoretical model, we employ two incompatible Pauli observables $\hat{\sigma}_x$ and $\hat{\sigma}_z$. Here, by means of two incompatible Pauli operators $\hat{\sigma}_x$ and $\hat{\sigma}_z$, the complementarity factor is found to be $c(\hat{\sigma}_x, \hat{\sigma}_z) = 1/2$ and the post-measurement states can be expressed as

$$\hat{\rho}_{\hat{\sigma}_x B} = \sum_i \left(\left|\hat{\sigma}_x^i\right\rangle\left\langle\hat{\sigma}_x^i\right| \otimes \boldsymbol{I}_B\right)\hat{\rho}_{AB}\left(\left|\hat{\sigma}_x^i\right\rangle\left\langle\hat{\sigma}_x^i\right| \otimes \boldsymbol{I}_B\right), \tag{14}$$
$$\hat{\rho}_{\hat{\sigma}_z B} = \sum_i \left(\left|\hat{\sigma}_z^i\right\rangle\left\langle\hat{\sigma}_z^i\right| \otimes \boldsymbol{I}_B\right)\hat{\rho}_{AB}\left(\left|\hat{\sigma}_z^i\right\rangle\left\langle\hat{\sigma}_z^i\right| \otimes \boldsymbol{I}_B\right), \tag{15}$$

where $\hat{I}_B$ is an identity operator in B's Hilbert space, $\left|\hat{\sigma}_x^i\right\rangle$ and $\left|\hat{\sigma}_z^i\right\rangle$ denote the eigenstates of operators $\hat{\sigma}_x$ and $\hat{\sigma}_z$, respectively. For coupled semiconductor charge qubits, employing the implicit form of the density matrix provided in Eq. (12), one can straightforwardly compute the post-measurement states.

$$\begin{aligned}\hat{\rho}_{\hat{\sigma}_x B} = \Bigg[&\frac{\hat{\rho}_{11}+\hat{\rho}_{33}}{2}\left(|ll\rangle\langle ll| + |rl\rangle\langle rl|\right) \\ &+\frac{\hat{\rho}_{22}+\hat{\rho}_{44}}{2}\left(|rr\rangle\langle rr| + |lr\rangle\langle lr|\right) \\ &+\frac{\hat{\rho}_{23}+\hat{\rho}_{41}}{2}\left(|rr\rangle\langle ll| + |lr\rangle\langle rl|\right) \\ &+\frac{\hat{\rho}_{14}+\hat{\rho}_{32}}{2}\left(|ll\rangle\langle rr| + |rl\rangle\langle lr|\right)\Bigg],\end{aligned} \tag{16}$$

$$\begin{aligned}\hat{\rho}_{\hat{\sigma}_z B} = &\left(\hat{\rho}_{11}|ll\rangle\langle ll| + \hat{\rho}_{22}|lr\rangle\langle lr|\right. \\ &\left.+\hat{\rho}_{33}|rl\rangle\langle rl| + \hat{\rho}_{44}|rr\rangle\langle rr|\right).\end{aligned} \tag{17}$$

The corresponding von Neumann entropies are

$$\mathcal{S}\left(\hat{\rho}_{\hat{\sigma}_x B}\right) = -\zeta_+\log_2\zeta_+ - \zeta_-\log_2\zeta_-, \tag{18}$$
$$\mathcal{S}\left(\hat{\rho}_{\hat{\sigma}_z B}\right) = \begin{pmatrix} -\hat{\rho}_{11}\log_2\hat{\rho}_{11} - \hat{\rho}_{22}\log_2\hat{\rho}_{22} \\ -\hat{\rho}_{33}\log_2\hat{\rho}_{33} - \hat{\rho}_{44}\log_2\hat{\rho}_{44} \end{pmatrix}, \tag{19}$$

where

$$\zeta_\pm = \frac{1}{4}\left(1 \pm \sqrt{\begin{bmatrix} 4(\hat{\rho}_{14}+\hat{\rho}_{32})(\hat{\rho}_{23}+\hat{\rho}_{41}) \\ +(\hat{\rho}_{11}-\hat{\rho}_{22}+\hat{\rho}_{33}-\hat{\rho}_{44})^2 \end{bmatrix}}\right). \tag{20}$$

The relevant entropies of $\hat{\rho}_B = \mathrm{Tr}_A\,\hat{\rho}_{AB}$ and $\hat{\rho}_{AB}$ are, respectively, obtained as

$$\mathcal{S}\left(\hat{\rho}_B\right) = \begin{bmatrix} -(\hat{\rho}_{11}+\hat{\rho}_{33})\log_2(\hat{\rho}_{11}+\hat{\rho}_{33}) \\ -(\hat{\rho}_{22}+\hat{\rho}_{44})\log_2(\hat{\rho}_{22}+\hat{\rho}_{44}) \end{bmatrix}, \tag{21}$$

$$\mathcal{S}\left(\hat{\rho}_{AB}\right) = -\sum_{i=1}^{4}\lambda_i\log_2\lambda_i, \tag{22}$$

where $\lambda_i \quad (i = 1,2,3,4)$ are the eigenvalues of the density matrix $\hat{\rho}(T)$, the eigenvalues of the state can be given by

$$\lambda_{1,2} = \frac{1}{2}\left(\hat{\rho}_{22}+\hat{\rho}_{33} \pm \sqrt{4\hat{\rho}_{23}\hat{\rho}_{32} + (\hat{\rho}_{22}-\hat{\rho}_{33})^2}\right),$$
$$\lambda_{3,4} = \frac{1}{2}\left(\hat{\rho}_{11}+\hat{\rho}_{44} \pm \sqrt{4\hat{\rho}_{14}\hat{\rho}_{41} + (\hat{\rho}_{11}-\hat{\rho}_{44})^2}\right). \tag{23}$$

Therefore, the entropic uncertainty (EUL) associated with the left-hand side of Eq. (3) becomes

$$\mathcal{U}_{\mathrm{L}} = \mathcal{S}\left(\hat{\rho}_{\sigma_x B}\right) + \mathcal{S}\left(\hat{\rho}_{\sigma_z B}\right) - 2\mathcal{S}\left(\hat{\rho}_B\right). \tag{24}$$

CPB Online In-Press

Meanwhile, we have that the lower bound (EUR) of the right-hand side of Eq. (3) is equal to

$$\mathcal{U}_{\mathrm{R}} = \mathcal{S}(\hat{\rho}_{AB}) - \mathcal{S}(\hat{\rho}_{B}) + \log_2 \frac{1}{c}, \tag{25}$$

$\mathcal{U}_{\mathrm{L}}$ and $\mathcal{U}_{\mathrm{R}}$ correspond to the QMA-EUR and the lower bound constraining Bob's estimation accuracy, respectively. In fact, the quantum memory information stored in B arises from the sum of $\mathcal{S}(\hat{\rho}_{\sigma_x B})$ and $\mathcal{S}(\hat{\rho}_{\sigma_z B})$, which determines the uncertainty of the measurement outcomes of $\hat{\sigma}_x$ and $\hat{\sigma}_z$.

To provide further insight into the dynamics of the relationship between QMA-EUR $\mathcal{U}_{\mathrm{L}}$ and the lower bound $\mathcal{U}_{\mathrm{R}}$, we introduce the tightness of QMA-EUR, which is a measure of the discrepancy between the two sides of inequality (3) and, as a result, is defined by[32]

$$\begin{aligned}\mathcal{U}_{\mathrm{T}} &= \mathcal{U}_{\mathrm{L}} - \mathcal{U}_{\mathrm{R}} \\ &= \mathcal{S}(\hat{\rho}_{\sigma_x B}) + \mathcal{S}(\hat{\rho}_{\sigma_z B}) - \mathcal{S}(\hat{\rho}_{B}) - \mathcal{S}(\hat{\rho}_{AB}) - \log_2 \frac{1}{c}.\end{aligned} \tag{26}$$

Smaller tightness values reveal higher consistency between QMA-EUR and the lower bound.

4. Quantifiers of quantum correlations

To investigate the characteristics of the relationship between the QMA-EUR and quantum correlation, we present two key quantifiers: EoF and QD.

4.1. Entanglement of formation

For a given density matrix, the EoF is evaluated through the concurrence[33] proposed by Wootters, which can be expressed as

$$\mathcal{E} = h\left(\frac{1+\sqrt{1-\mathcal{C}^2}}{2}\right), \tag{27}$$

where $h(x) = -x\log_2 x - (1-x)\log_2(1-x)$. For the thermal equilibrium state Eq. (14), the expression of the concurrence can be written as

$$\mathcal{C} = 2\max[0, |\hat{\rho}_{23}| - \sqrt{\hat{\rho}_{11}\hat{\rho}_{44}}, |\hat{\rho}_{14}| - \sqrt{\hat{\rho}_{22}\hat{\rho}_{33}}]. \tag{28}$$

4.2. Quantum discord

QD, which is the difference between the total amount of correlation and the classical correlation (CC), is defined as follows:

$$\mathcal{D}(\hat{\rho}_{AB}) = \mathcal{I}(\hat{\rho}_{AB}) - \mathcal{C}(\hat{\rho}_{AB}). \tag{29}$$

The total correlation of a bipartite quantum system is quantified by quantum mutual information (QMI)

$$\mathcal{I}(\hat{\rho}_{AB}) = \mathcal{S}(\hat{\rho}_{A}) + \mathcal{S}(\hat{\rho}_{B}) - \mathcal{S}(\hat{\rho}_{AB}), \tag{30}$$

where $\mathcal{S}(\hat{\rho}_{AB}) = -\mathrm{Tr}(\hat{\rho}_{AB}\log_2\hat{\rho}_{AB})$ is the von Neumann entropy, and $\hat{\rho}_{A(B)} = \mathrm{Tr}_{B(A)}\hat{\rho}_{AB}$ is the reduced density operator of the subsystems. Classical correlation was first proposed by Ollivier and Zurek,[34] and later Henderson and Vedral offered an explicit interpretation[35]

$$\mathcal{C}(\hat{\rho}_{AB}) = S(\hat{\rho}_{A}) - \mathcal{M}(\hat{\rho}_{AB}), \tag{31}$$

where $\mathcal{M}(\hat{\rho}_{AB}) = \min_{\{\Pi_k\}} \mathcal{S}(\hat{\rho}_{AB}|\{\Pi_k\})$ is the minimum conditional entropy (MCE), which can be written as[36]

$$\mathcal{M}(\hat{\rho}_{AB}) = -M_+\log_2 M_+ - M_-\log_2 M_-, \tag{32}$$

where

$$\begin{aligned}M_+ &= \frac{1}{2}\left(1+\sqrt{(\hat{\rho}_{11}-\hat{\rho}_{44})^2 + (\hat{\rho}_{14}+\hat{\rho}_{23})^2}\right), \\ M_- &= \frac{1}{2}\left(1-\sqrt{(\hat{\rho}_{11}-\hat{\rho}_{44})^2 + (\hat{\rho}_{14}+\hat{\rho}_{23})^2}\right).\end{aligned} \tag{33}$$

To further investigate the dynamics of uncertainty, combining Eqs. (25), (29), and (31), one can obtain the intrinsic link between the bound of measured uncertainty and QD

$$\mathcal{U}_{\mathrm{R}} = \log_2 \frac{1}{c} - \mathcal{D}(\hat{\rho}_{AB}) + \mathcal{M}(\hat{\rho}_{AB}). \tag{34}$$

Equation (34) reveals a relationship that provides insight into the dynamical behaviors of the lower bound ($\mathcal{U}_{\mathrm{R}}$), which depends on QD $\mathcal{D}(\hat{\rho}_{AB})$ and MCE $\mathcal{M}(\hat{\rho}_{AB})$.

5. Results and discussion

In this section, we illustrate the impact of various physical parameters, namely equilibrium temperature (T), coupling strength (J), tunneling coupling energy (TCE) Δ_1, and TCE ratio Δ_1/Δ_2, on the dynamical evolution of the QMA-EUR and quantum correlations. The impact of these parameters can be observed in the figures presented below. First, we investigate how the equilibrium temperature (T) affects the evolution of the QMA-EUR and quantum correlations in the system, as shown in Fig. 2

As shown in Fig. 2, the QMA-EUR ($\mathcal{U}_{\mathrm{L}}$) and its lower bound ($\mathcal{U}_{\mathrm{R}}$) monotonously increase all the time with the growth of the temperature T. However, as the temperature continues to rise further, the two bounds of the QMA-EUR ($\mathcal{U}_{\mathrm{L}}$) and its lower bound ($\mathcal{U}_{\mathrm{R}}$) gradually reach their maximum value ($\mathcal{U}_{\mathrm{L}} = \mathcal{U}_{\mathrm{R}} = 2$). The characteristics of tightness $\mathcal{U}_{\mathrm{T}}$ demonstrate the discrepancy between QMA-EUR $\mathcal{U}_{\mathrm{L}}$ and the lower bound $\mathcal{U}_{\mathrm{R}}$ of the uncertainty inequality. The tightness $\mathcal{U}_{\mathrm{T}}$ is null for near-zero temperatures, and then proceeds to rise before eventually decreasing and vanishing as the QMA-EUR ($\mathcal{U}_{\mathrm{L}}$) and its lower bound ($\mathcal{U}_{\mathrm{R}}$) become overlapped for high temperatures T.

CPB Online In-Press

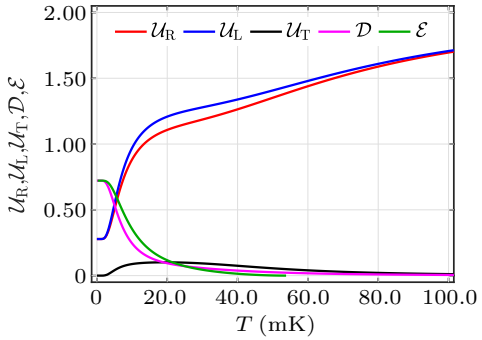


Fig. 2. Variations of EoF $\mathcal{E}$ (green curve), QD $\mathcal{D}$ (magenta curve), the components of the QMA-EUR $\mathcal{U}_L$ (blue curve), the bound $\mathcal{U}_R$ (red curve), and their tightness $\mathcal{U}_T$ (black curve) as functions of the temperature T. The values of parameters $\varepsilon_1 = \varepsilon_2 = 0$, $J = 25$ μeV, $\Delta_1 = J/4$ and $\Delta_2 = J/8$.

The decoherence is displayed clearly in the behavior of the EoF $\mathcal{E}$ and QD $\mathcal{D}$, where the EoF $\mathcal{E}$ decreases faster than QD $\mathcal{D}$ as the temperature increases and completely vanishes at $T_{\mathcal{E}} > 53.9$ mK, though the latter is more resistant than the former because it relatively survives longer. Furthermore, as shown in Fig. 2, there exists a critical temperature $T_C \approx 1.3566$ mK at which the QMA-EUR $\mathcal{U}_L$ overlaps with the lower bound $\mathcal{U}_R$. When the temperature is constrained with $T > T_C$, the QMA-EUR $\mathcal{U}_L$ is greater than its lower bound $(\mathcal{U}_R)$. For $T < T_C$, the QMA-EUR $\mathcal{U}_L$ and its lower bound $(\mathcal{U}_R)$ maintain fixed values $\mathcal{U}_L^{\min} = \mathcal{U}_R^{\min} = 0.2781$. The EoF $\mathcal{E}$ and QD $\mathcal{D}$ stabilize at maximum values $\mathcal{E}_{\max} = \mathcal{D}_{\max} = 0.7219$. Based on this observation, it can be inferred that lower temperatures tend to facilitate more precise measurements. The higher temperature of a quadruple quantum dot device for two charge qubits can lead to the inflation of the uncertainty.

Figure 3 shows that the EoF $(\mathcal{E})$ and QD $(\mathcal{D})$ are absent when the strength of coupling J is zero for several values of parameters $\varepsilon_1 = \varepsilon_2 = 0$, $T = 10$ mK, $\Delta_1 = J/4$ and $\Delta_2 = J/8$. This result shows that the strength of coupling J can be used to either turn on or off the entanglement and quantum correlations. As shown in Fig. 3, the magnitudes of the EoF $(\mathcal{E})$ and QD $(\mathcal{D})$ initially take zero values, and then display an increasing behavior until they reach a threshold value J_{th}, after which they decrease but never vanish, even for stronger values of the strength of coupling J. It is clear that the strength of coupling J between the two charge qubits has to be adjusted to a specific interval to utilize quantum correlations for better resourcefulness in a quadruple quantum dot device for two charge qubits state.

One can obtain that the strength of coupling J can reduce the QMA-EUR $(\mathcal{U}_L)$ and its lower bound $(\mathcal{U}_R)$, as can be seen from Fig. 3. We see that the presence of a strength of coupling J hinders the negative impact of growing temperature T, which tends to increase the QMA-EUR $(\mathcal{U}_L)$ and its lower bound $(\mathcal{U}_R)$. The QMA-EUR $(\mathcal{U}_L)$ will shrink into the lower bound $(\mathcal{U}_R)$ with the increase of the strength of coupling J. The minimum values of the QMA-EUR $(\mathcal{U}_L)$, its lower bound $(\mathcal{U}_R)$, and the maximum tightness $(\mathcal{U}_T)$ do not match. We find that the QMA-EUR $(\mathcal{U}_L)$ and its lower bound $(\mathcal{U}_R)$ first increase, then decrease, and finally increase with the increase of the strength of coupling J, as displayed in Fig. 3. It is worth noting that the QMA-EUR $(\mathcal{U}_L)$ and its lower bound $(\mathcal{U}_R)$ have some fluctuations, which are not fully synchronous with the systematic QD $(\mathcal{D})$.

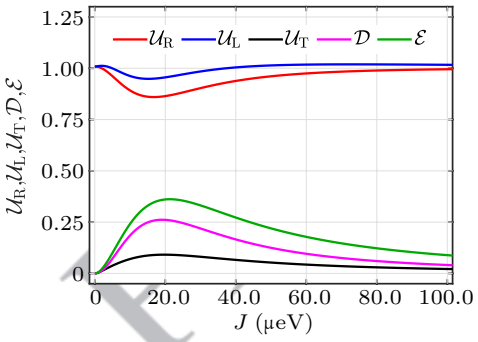


Fig. 3. Variations of EoF $\mathcal{E}$ (green curve), QD $\mathcal{D}$ (magenta curve), the components of the QMA-EUR $\mathcal{U}_L$ (blue curve), the bound $\mathcal{U}_R$ (red curve), and their tightness $\mathcal{U}_T$ (black curve) as functions of the strength of coupling J. The values of parameters $\varepsilon_1 = \varepsilon_2 = 0$, $T = 10$ mK, $\Delta_1 = J/4$ and $\Delta_2 = J/8$.

Now, let us turn to explore the relationship among the QMA-EUR $(\mathcal{U}_L)$, lower bound $(\mathcal{U}_R)$, QD $(\mathcal{D})$, and TCE Δ_1, as plotted in Fig. 4. It is obvious that the QMA-EUR $(\mathcal{U}_L)$ and its lower bound $(\mathcal{U}_R)$ first increase, then decrease, and finally increase with the growing Δ_1, while the quantum correlation first increases and then decreases with the increasing Δ_1. It can be observed that the values of QMA-EUR and its lower bound $\mathcal{U}_L = \mathcal{U}_R = 1.04287$, when the system state is separable (i.e., when the EoF is zero) in the case of $\Delta_1 = 0$. As the parameter Δ_1 increases, QMA-EUR and its lower bound attain their respective maximum values $\mathcal{U}_L^{\max} = 1.1137$ and $\mathcal{U}_R^{\max} = 1.0894$. As the parameter Δ_1 continues to increase further, both QMA-EUR and its lower bound then decrease to their respective minimum peak values $\mathcal{U}_L^{\min} = 0.8560$ and $\mathcal{U}_R^{\min} = 0.7682$. It is worth noting that the QMA-EUR $(\mathcal{U}_L)$ and lower bound $(\mathcal{U}_R)$ will saturate into a fixed value as the value of Δ_1 becomes large enough.

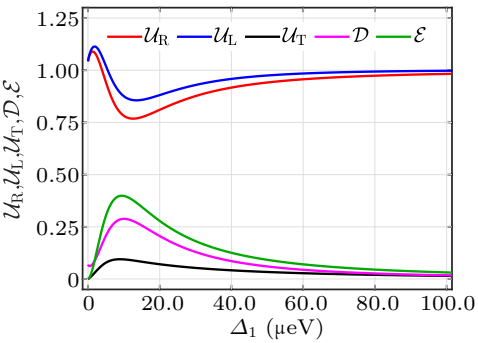


Fig. 4. Variations of EoF $\mathcal{E}$ (green curve), QD $\mathcal{D}$ (magenta curve), the components of the QMA-EUR $\mathcal{U}_L$ (blue curve), the lower bound $\mathcal{U}_R$ (red curve), and their tightness $\mathcal{U}_T$ (black curve) as functions of the TCE Δ_1. The values of parameters $\varepsilon_1 = \varepsilon_2 = 0$, $T = 10$ mK, $J = 25$ μeV and $\Delta_2 = J/8$.

CPB Online First

In order to study the effects of the TCE $\Delta_{i=1,2}$ on the quantum correlations, we plot the behavior of QMA-EUR ($\mathcal{U}_{\rm L}$), lower bound ($\mathcal{U}_{\rm R}$), and QD ($\mathcal{D}$) as a function of the TCE ratio Δ_1/Δ_2 in Fig. 5. We can observe that the EoF $\mathcal{E}$ vanishes when the TCE ratio $\Delta_1/\Delta_2 = 0$, regardless of the values of the TCE $\Delta_{i=1,2}$. In this scenario, the quadruple quantum dot device for two charge qubits does not exhibit entanglement because electrons can no longer undergo intra-device movement within the quadruple quantum dot structure. On the other hand, QD ($\mathcal{D}$) is still present although the value of the TCE ratio $\Delta_1/\Delta_2 = 0$, which shows again that, despite the state being separable, the system still possesses quantum correlation. It should be emphasized that the EoF $\mathcal{E}$ can be either greater than or less than QD ($\mathcal{D}$) when considering smaller values of the TCE ratio Δ_1/Δ_2. Furthermore, according to the numerical results in Fig. 5, one can conjecture that the TCE ratio Δ_1/Δ_2 is able to effectively reduce the entropic uncertainty and improve the quantum correlation in some specific ratios. Taking this into account, appropriate control of $(\Delta_{i=1,2}, \Delta_1/\Delta_2)$ is critical for reducing uncertainties and enhancing quantum correlations in practical scenarios.

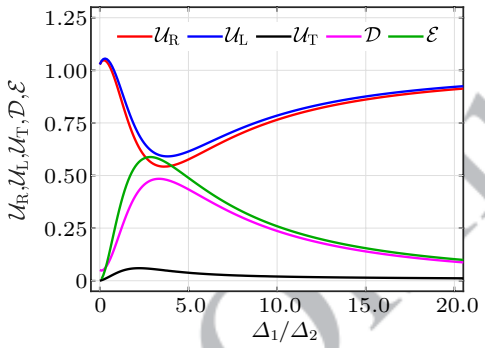


Fig. 5. Variations of EoF $\mathcal{E}$ (green curve), QD $\mathcal{D}$ (magenta curve), the components of the QMA-EUR $\mathcal{U}_{\rm L}$ (blue curve), the bound $\mathcal{U}_{\rm R}$ (red curve), and their tightness $\mathcal{U}_{\rm T}$ (black curve) as functions of the TCE ratio Δ_1/Δ_2. The values of parameters $\varepsilon_1 = \varepsilon_2 = 0$, $T = 5$ mK, $J = 25$ μeV and $\Delta_2 = J/10$.

By comparing the results from Figs. 3–5, we can observe that the behavior of EoF $\mathcal{E}$, QD $\mathcal{D}$, QMA-EUR $\mathcal{U}_{\rm L}$, lower bound $\mathcal{U}_{\rm R}$, and tightness $\mathcal{U}_{\rm T}$ is similarly impacted by both the strength of coupling J, TCE $\Delta_{i=1,2}$, and TCE ratio Δ_1/Δ_2 in a quadruple quantum dot device for two charge qubits. Obviously, one can find that, as shown in Figs. 2–5, the variation of QD ($\mathcal{D}$) is almost opposite to the variation of the lower bound ($\mathcal{U}_{\rm R}$), which is essentially in agreement with the outcome from Eq. (30). This is because the magnitude of the uncertainty bound is determined by both QD ($\mathcal{D}$) and the MCE $\mathcal{M}(\hat{\rho}_{AB})$, which exhibit the natural competition while quantifying the uncertainty. This reflects that the dominant gradient is the QD ($\mathcal{D}$) rather than the MCE $\mathcal{M}(\hat{\rho}_{AB})$. Based on these, we can infer that MCE $\mathcal{M}(\hat{\rho}_{AB})$ plays a leading role in this scenario.

In practice, our scheme is highly suitable for experimental implementation. The non-Markovian effects on coherence and entanglement in a quadruple quantum dot system coupled to bosonic reservoirs can be investigated by directly measuring the population of a qubit, eliminating the need for tomographic reconstruction of the density matrix. Moreover, our approach does not require specific knowledge of the interaction between the qubit and the reservoir. These favorable features render our scheme experimentally feasible, both in realistic settings[37,38] and in simulated environments.[39–41]

6. Conclusion

To summarize, we have investigated the dynamics of the QMA-EUR and its lower bounds in a quadruple quantum dot device for two charge qubits under intrinsic decoherence. In particular, we explored the dynamical evolution of the entropic uncertainty with the complementary measurement pair $(\hat{\sigma}_x, \hat{\sigma}_z)$ under the influence of temperature, coupling strength, TCE, and the TCE ratio. It has been verified that equilibrium temperature significantly impacts quantum properties: higher temperatures erode entanglement and nonlocal correlations while increasing QMA-EUR. Intriguingly, our results have confirmed the existence of optimized parameters that govern both the coupling strength and the ratio of TCE. These parameters enable effective uncertainty reduction via quantum weak measurement, which is highly desirable for practical quantum information processing. Therefore, we believe our observations may offer novel insights into the dynamics of entropic uncertainty in a quadruple quantum dot device for two charge qubits, and contribute to illuminating quantum precision measurement across diverse solid-state systems.

Acknowledgement

This work is supported by University-Industry Collaborative Education Program (Grant No. 220506627183928).

References

[1] Heisenberg W 1927 *Z. Phys.* **43** 172
[2] Kennard E H 1927 *Z. Phys.* **44** 326
[3] Robertson H P 1929 *Phys. Rev.* **34** 163
[4] Deutsch D 1983 *Phys. Rev. Lett.* **50** 631
[5] Kraus K 1987 *Phys. Rev. D* **35** 3070
[6] Maassen H and Uffink J B M 1988 *Phys. Rev. Lett.* **60** 1103
[7] Renes J M and Boileau J C 2009 *Phys. Rev. Lett.* **103** 020402
[8] Li C F, Xu J S, Xu X Y, *et al.* 2011 *Nat. Phys.* **7** 752
[9] Prevedel R, Hamel D, Colbeck R, *et al.* 2011 *Nat. Phys.* **7** 757
[10] Ming F, Wang D, Fan X G, *et al.* 2020 *Phys. Rev. A* **102** 012606
[11] Bergh B and Garttner M 2021 *Phys. Rev. A* **103** 052412
[12] Song M L, Li L J, Song X K, *et al.* 2022 *Phys. Rev. E* **106** 054107
[13] Hosseiny S M, Seyed-Yazdi J and Norouzi M 2024 *Sci. Rep.* **14** 26033
[14] Lee K Y, Lin J D, Lemr K, *et al.* 2025 *npj Quantum Inform.* **11** 72
[15] Maroulakos D, Jasiukiewicz C, Wal A, *et al.* 2025 *Phys. Rev. B* **111** 224426
[16] Coles P J, Berta M, Tomamichel M, *et al.* 2017 *Rev. Mod. Phys.* **89** 015002
[17] Wang R and Chau H F 2025 *Phys. Rev. Lett.* **135** 020801
[18] Brandner K and Saito K 2025 *Phys. Rev. Lett.* **135** 046302
[19] Gühne O and Lewenstein M 2004 *Phys. Rev. A* **70** 022316
[20] Ali H, Basit A and Li P B 2025 *Phys. Rev. A* **111** 032418
[21] Zhang D J, Liu C L, Yu X D, *et al.* 2018 *Phys. Rev. Lett.* **120** 170501

CPB Online In Press

[22] Lu X M and Wang X 2021 *Phys. Rev. Lett.* **126** 120503
[23] Chen X Y, Zhang N N, He W T, *et al*. 2022 *npj Quantum Inf.* **8** 22
[24] Zhang D J and Tong D M 2024 *Phys. Rev. Lett.* **133** 040202
[25] Zhang D J and Tong D M 2025 *Phys. Rev. Lett.* **134** 110802
[26] Shinkai G, Hayashi T, Ota T and Fujisawa T 2009 *Phys. Rev. Lett.* **103** 056802
[27] Hayashi T, Fujisawa T, Cheong H D, *et al*. 2003 *Phys. Rev. Lett.* **91** 226804
[28] Shinkai G, Hayashi T, Hirayama Y, *et al*. 2007 *Appl. Phys. Lett.* **90** 103116
[29] Fujisawa T, Shinkai G, Hayashi T and Ota T 2011 *Physica E* **43** 730
[30] Ait Mansour H, Faqir M and El Baz M 2023 *Int. J. Theor. Phys.* **62** 58
[31] Wang H 2025 *Quantum Inf. Process.* **24** 153
[32] Rahman A U, Zidan N, Zangi S M, *et al*. 2022 *Quantum Inf. Process.* **21** 354
[33] Wootters W K 1998 *Phys. Rev. Lett.* **80** 2245
[34] Ollivier H and Zurek W H 2001 *Phys. Rev. Lett.* **88** 017901
[35] Henderson L and Vedral V 2001 *J. Phys. A: Math. Gen.* **34** 6899
[36] Wang H 2025 *Appl. Phys. A* **131** 641
[37] Vahala K J 2003 *Nature* **424** 839
[38] Lee I S, Filatov M and Min S K 2025 *Nat. Commun.* **16** 4554
[39] Georgescu I M, Ashhab S and Nori F 2014 *Rev. Mod. Phys.* **86** 153
[40] Sun K, Kang M, Nuomin H, *et al*. 2025 *Nat. Commun.* **16** 4042
[41] Porras D, Marquardt F, Von Delft J, *et al*. 2008 *Phys. Rev. A* **78** 010101

CPB Online In-Press